

Uncertainty-informed Mutual Learning for Joint Medical Image Classification and Segmentation

Kai Ren^{1,2,*}, Ke Zou^{1,2,*}, Xianjie Liu², Yidi Chen³, Xuedong Yuan^{1,2,✉},
Xiaojing Shen^{1,4}, Meng Wang⁵, Huazhu Fu^{5,✉}

¹ National Key Laboratory of Fundamental Science on Synthetic Vision,
Sichuan University, Sichuan, China

² College of Computer Science, Sichuan University, Sichuan, China

³ Department of Radiology, West China Hospital, Sichuan University, Sichuan, China

⁴ College of Mathematics, Sichuan University, Sichuan, China

⁵ Institute of High Performance Computing, Agency for Science, Technology and
Research, Singapore

yxd@scu.edu.cn;hzfu@ieee.org

Abstract. Classification and segmentation are crucial in medical image analysis as they enable accurate diagnosis and disease monitoring. However, current methods often prioritize the mutual learning features and shared model parameters, while neglecting the reliability of features and performances. In this paper, we propose a novel Uncertainty-informed Mutual Learning (UML) framework for reliable and interpretable medical image analysis. Our UML introduces reliability to joint classification and segmentation tasks, leveraging mutual learning with uncertainty to improve performance. To achieve this, we first use evidential deep learning to provide image-level and pixel-wise confidences. Then, an uncertainty navigator is constructed for better using mutual features and generating segmentation results. Besides, an uncertainty instructor is proposed to screen reliable masks for classification. Overall, UML could produce confidence estimation in features and performance for each link (classification and segmentation). The experiments on the public datasets demonstrate that our UML outperforms existing methods in terms of both accuracy and robustness. Our UML has the potential to explore the development of more reliable and explainable medical image analysis models.

Keywords: Mutual learning · Medical image classification and segmentation · Uncertainty estimation

1 Introduction

Accurate and robust classification and segmentation of the medical image are powerful tools to inform diagnostic schemes. In clinical practice, the image-level classification and pixel-wise segmentation tasks are not independent [8,27]. Joint

* denotes equal contribution.

classification and segmentation can not only provide clinicians with results for both tasks simultaneously, but also extract valuable information and improve performance. However, improving the reliability and interpretability of medical image analysis is still reaching.

Considering the close correlation between the classification and segmentation, many researchers [6, 8, 20, 22, 24, 27, 28] proposed to collaboratively analyze the two tasks with the help of sharing model parameters or task interacting. Most of the methods are based on sharing model parameters, which improves the performance by fully utilizing the supervision from multiple tasks [8, 27]. For example, Thomas *et al.* [20] combined whole image classification and segmentation of skin cancer using a shared encoder. Task interacting is also a widely used method [12, 24, 28] as it can introduce the high-level features and results produced by one task to benignly guide another. However, there has been relatively little research on introducing reliability into joint classification and segmentation. The reliability and interpretability of the model are particularly important for clinical tasks, a single result of the most likely hypothesis without any clues about how to make the decision might lead to misdiagnoses and sub-optimal treatment [10, 22]. One potential way of improving reliability is to introduce uncertainty for the medical image analysis model.

The current uncertainty estimation method can roughly include the Dropout-based [11], ensemble-based [4, 18, 19], deterministic-based methods [21] and evidential deep learning [5, 16, 23, 30, 31]. All of these methods are widely utilized in classification and segmentation applications for medical image analysis. Abdar *et al.* [1] employed three uncertainty quantification methods (Monte Carlo dropout, Ensemble MC dropout, and Deep Ensemble) simultaneously to deal with uncertainty estimation during skin cancer image classification. Zou *et al.* [31] proposed TBraTS based on evidential deep learning to generate robust segmentation results for brain tumor and reliable uncertainty estimations. Unlike the aforementioned methods, which only focus on uncertainty in either medical image classification or segmentation. Furthermore, none of the existing methods have considered how pixel-wise and image-level uncertainty can help improve performance and reliability in mutual learning.

Based on the analysis presented above, we design a novel Uncertainty-informed Mutual Learning (UML) network for medical image analysis in this study. Our UML not only enhances the image-level and pixel-wise reliability of medical image classification and segmentation, but also leverages mutual learning under uncertainty to improve performance. Specifically, we adopt evidential deep learning [16, 31] to simultaneously estimate the uncertainty of both to estimate image-level and pixel-wise uncertainty. We introduce an Uncertainty Navigator for segmentation (UN) to generate preliminary segmentation results, taking into account the uncertainty of mutual learning features. We also propose an Uncertainty Instructor for classification (UI) to screen reliable masks for classification based on the preliminary segmentation results. Our UML represents pioneering work in introducing reliability and interpretability to joint classification and seg-

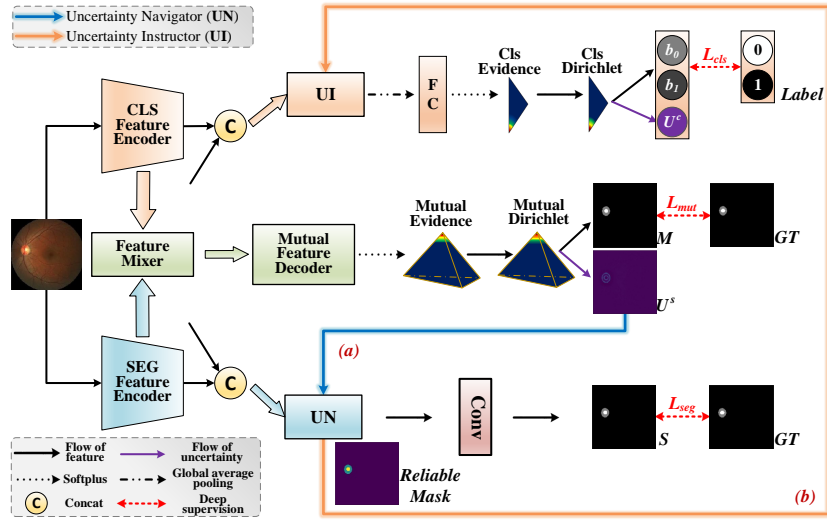


Fig. 1. The framework of Uncertainty-informed Mutual Learning network.

mentation, which has the potential to the development of more trusted medical analysis tools.

2 Method

The overall architecture of the proposed UML, which leverages mutual learning under uncertainty, is illustrated in Fig. 1. Firstly, Uncertainty Estimation for Classification and Segmentation adapts evidential deep learning to provide image-level and pixel-wise uncertainty. Then, Trusted Mutual Learning not only utilizes the proposed UN to fully exploit pixel-wise uncertainty as the guidance for segmentation but also introduces the UI to filter the feature flow between task interaction.

Given an input medical image $I, I \in \mathbb{R}^{H,W}$, where H, W are the height and width of the image, separately. To maximize the extraction of specific information required for two different tasks while adequately mingling the common feature which is helpful for both classification and segmentation, I is firstly fed into the dual backbone network that outputs the classification feature maps $f_i^c, i \in 1, \dots, 4$ and segmentation feature maps $f_i^s, i \in 1, \dots, 4$, where i denotes the i^{th} layer of the backbone. Then following [29], we construct the Feature Mixer using Pairwise Channel Map Interaction to mix the original feature and get the mutual feature maps $f_i^m, i \in 1, \dots, 4$. Finally, we combine the last layer of mutual feature with the original feature.

Our code has been released in <https://github.com/KarryRen/UML>.

2.1 Uncertainty Estimation for Classification and Segmentation

Classification Uncertainty Estimation. For the K classification problems, we utilize Subjective Logic [7] to produce the belief mass of each class and the uncertainty mass of the whole image based on *evidence*. Accordingly, given a classification result, its $K + 1$ mass values are all non-negative and their sum is one:

$$\sum_{k=1}^K b_k^c + U^c = 1, \quad (1)$$

where $b_k^c \geq 0$ and $U^c \geq 0$ denote the probability belonging to the k^{th} class and the overall uncertainty value, respectively. As shown in Fig. 1, the *cls evidence* $e^c = [e_1^c, \dots, e_K^c]$ for the classification result is acquired by an activation function layer softplus and $e_k^c \geq 0$. Then the *cls Dirichlet* distribution can be parameterize by $\alpha^c = [\alpha_1^c, \dots, \alpha_K^c]$, which associated with the *cls evidence* e_k^c , *i.e.* $\alpha_k^c = e_k^c + 1$. In the end, the image-level belief mass and the uncertainty mass of the classification can be calculated by

$$b_k^c = \frac{e_k^c}{T^c} = \frac{\alpha_k^c - 1}{T^c}, \text{ and } U^c = \frac{K}{T^c}, \quad (2)$$

where $T^c = \sum_{k=1}^K \alpha_k^c = \sum_{k=1}^K (e_k^c + 1)$ represents the Dirichlet strength. Actually, Eq. 2 describes such a phenomenon that the higher the probability assigned to the k^{th} class, the more evidence observed for k^{th} category should be.

Segmentation Uncertainty Estimation. Essentially, segmentation is the classification for each pixel of a medical image. Given a pixel-wise segmentation result, following [31] the *seg Dirichlet* distribution can be parameterized by $\alpha^{s(h,w)} = [\alpha_1^{s(h,w)}, \dots, \alpha_Q^{s(h,w)}]$, $(h, w) \in (H, W)$. We can compute the belief mass and uncertainty mass of the input image by

$$b_q^{s(h,w)} = \frac{e_q^{s(h,w)}}{T^{s(h,w)}} = \frac{\alpha_q^{s(h,w)} - 1}{T^{s(h,w)}}, \text{ and } u^{s(h,w)} = \frac{Q}{T^{s(h,w)}}, \quad (3)$$

where $b_q^{s(h,w)} \geq 0$ and $u^{s(h,w)} \geq 0$ denote the probability of the pixel at coordinate (h, w) for the q^{th} class and the overall uncertainty value respectively. We also define $U^s = \{u^{s(h,w)}, (h, w) \in (H, W)\}$ as the pixel-wise uncertainty of the segmentation result.

2.2 Uncertainty-informed Mutual Learning

Uncertainty Navigator for Segmentation. Actually, we have already obtained an initial segmentation mask $M = \alpha^s$, $M \in (Q, H, W)$ through estimating segmentation uncertainty, and achieved lots of valuable features such as lesion location. In our method, appropriate uncertainty guided decoding on the feature list can obtain more reliable information and improve the performance of segmentation [3, 9, 26]. So we introduce Uncertainty Navigator for Segmentation(UN) as a feature decoder, which incorporates the pixel-wise uncertainty

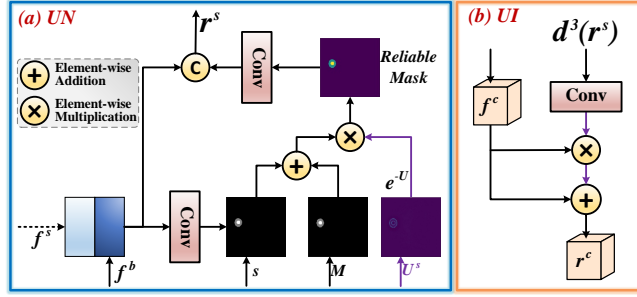


Fig. 2. Details of (a) Uncertainty Navigator (UN) and (b) Uncertainty Instructor (UI).

in U^s and lesion location information in M with the segmentation feature maps to generate the segmentation result and reliable features. Having a UNet-like architecture [15], UN computes segmentation $s_i, i \in 1, \dots, 4$ at each layer, as well as introduces the uncertainty in the bottom and top layer by the same way. Take the top layer as an example, as shown in Fig. 2 (a), UN calculates the reliable mask M^r by:

$$M^r = (s_1 \oplus M) \otimes e^{-U^s}, \quad (4)$$

Then, the reliable segmentation feature r^s , which combines the trusted information in M^r with the original features, is generated by:

$$r^s = \text{Cat}(\text{Conv}(M^r), \text{Cat}(f_1^s, f_2^b)), \quad (5)$$

where f_1^s derives from jump connecting and f_2^b is the feature of the s_2 with one up-sample operation. $\text{Conv}(\cdot)$ represents the convolutional operation, $\text{Cat}(\cdot, \cdot)$ denotes the concatenation. Especially, the U^s is also used to guide the bottom feature with the dot product. The r^s is calculated from the segmentation result s_1 and contains uncertainty navigated information not found in s_1 .

Uncertainty Instructor for Classification. In order to mine the complementary knowledge of segmentation as the instruction for the classification and eliminate intrusive features, we devise an Uncertainty Instructor for classification (UI) following [22]. Fig. 2 (b) shows the architecture of UI. It firstly generates reliable classification features r^c fusing the initial classification feature maps f_4^c and the rich information (e.g., lesion location and boundary characteristic) in r^s , which can be expressed by:

$$r^c = f_4^c \oplus (\text{Conv}(d^3(r^s)) \otimes f_4^c), \quad (6)$$

where $d^n(\cdot)$ denotes that the frequency of down-sampling operations is n . Then the produced features are transformed into a semantic feature vector by the global average pooling. The obtained vector is converted into the final result (belief values) of classification with uncertainty estimation.

2.3 Mutual Learning Process

In a word, to obtain the final results of classification and segmentation, we construct an end-to-end mutual learning process, which is supervised by a joint loss function. To obtain an initial segmentation result M and a pixel-wise uncertainty estimation U^s , following [31], a mutual loss is used as:

$$\mathcal{L}_m(\alpha^s, y^s) = \mathcal{L}_{ice}(\alpha^s, y^s) + \lambda_1^m \mathcal{L}_{KL}(\alpha^s) + \lambda_2^m \mathcal{L}_{Dice}(\alpha^s, y^s), \quad (7)$$

where y^s is the Ground Truth (GT) of the segmentation. The hyperparameters λ_1^m and λ_2^m play a crucial role in controlling the Kullback-Leibler divergence (KL) and Dice score, as supported by [31]. Similarly, in order to estimate the image-level uncertainty and classification results, a classification loss is constructed following [5], as:

$$\mathcal{L}_c(\alpha^c, y^c) = \mathcal{L}_{ace}(\alpha^c, y^c) + \lambda^c \mathcal{L}_{KL}(\alpha^c), \quad (8)$$

where y^c is the true class of the input image. The hyperparameter λ^c serves as a crucial hyperparameter governing the KL, aligning with previous work [5]. To obtain reliable segmentation results, we also adopt deep supervision for the final segmentation result $S = \{s_i, i = 1, \dots, 4\}$, which can be denoted as:

$$\mathcal{L}_s = \frac{\sum_{i=1}^4 \mathcal{L}_{Dice}(v^{i-1}(s_i), y^s)}{4}, \quad (9)$$

where v^n indicates the number of up-sampling is 2^n . Thus, the overall loss function of our UML can be given as:

$$\mathcal{L}_{UML}(\alpha^s, \alpha^c, y^s, y^c) = w^m \mathcal{L}_m(\alpha^s, y^s) + w^c \mathcal{L}_c(\alpha^c, y^c) + w^s \mathcal{L}_s, \quad (10)$$

where w^m, w^c, w^s denote the weights and are set 0.1, 0.5, 0.4, separately.

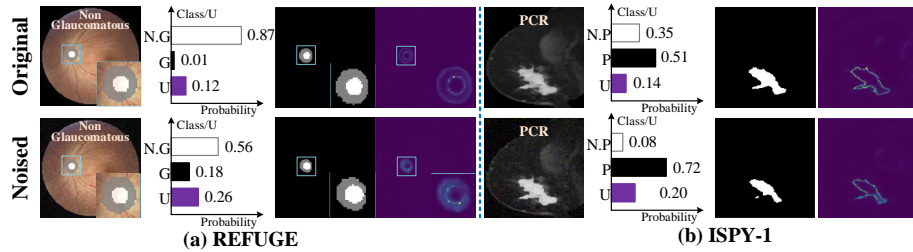
3 Experiments

Dataset & Implementation. We evaluate the our UML network on two datasets REFUGE [14] and ISPY-1 [13]. REFUGE contains two tasks, classification of glaucoma and segmentation of optic disc/cup in fundus images. The overall 1200 images were equally divided for training, validation, and testing. All images are uniformly adjusted to 256×256 pixels. The tasks of ISPY-1 are the pCR prediction and the breast tumor segmentation. A total of 157 patients who suffer the breast cancer are considered - 43 achieve pCR and 114 non-pCR. For each case, we cut out the slices in the 3D image and totally got 1,570 2D images, which are randomly divided into the train, validation, and test datasets with 1,230, 170, and 170 slices, respectively.

We implement the proposed method via PyTorch and train it on NVIDIA GeForce RTX 2080Ti. The Adam optimizer is adopted to update the overall parameters with an initial learning rate 0.0001 for 100 epochs. The scale of the

Table 1. Evaluation of the classification and segmentation performance. The top-2 results are highlighted in bold and underlined ($p \leq 0.01$).

Method		REFUGE						ISPY-1			
		CLS		SEG				CLS		SEG	
		<i>ACC</i>	<i>F1</i>	<i>DI_{disc}</i>	<i>ASSD_{disc}</i>	<i>DI_{cup}</i>	<i>ASSD_{cup}</i>	<i>ACC</i>	<i>F1</i>	<i>DI</i>	<i>ASSD</i>
Single-task	EC	0.560	0.641	\	\	\	\	0.735	0.648	\	\
	TBraTS	\	\	0.776	1.801	0.787	1.798	\	\	0.784	4.075
	TransUNet	\	\	0.633	2.807	0.628	2.638	\	\	0.692	5.904
Multi-task	BCS	0.723	0.778	<u>0.802</u>	<u>1.692</u>	<u>0.831</u>	<u>1.532</u>	<u>0.758</u>	<u>0.692</u>	0.773	3.804
	DSI	<u>0.838</u>	<u>0.834</u>	0.793	2.030	0.811	1.684	0.741	0.673	0.760	4.165
	Ours	0.853	0.875	0.855	1.560	0.858	1.251	0.771	0.713	0.785	<u>3.927</u>

**Fig. 3.** The visual result of segmentation and classification in REFUGE and ISPY-1. Top is the original image, and bottom is the input with Gaussian noise ($\sigma = 0.05$). From left to right, input (with GT), the result of classification (belief and image-level uncertainty), the result of segmentation, pixel-wise uncertainty.

regularizer is set as 1×10^{-5} . We choose VGG-16 and Res2Net as the encoders for classification and segmentation, separately.

Compared Methods & Metrics. We compared our method with single-task methods and multi-task methods. (1) Single-task methods: (a) EC [17], (b) TBraTS [31] and (c) TransUNet [2]. Evidential deep learning for classification (EC) first proposed to parameterize classification probabilities as Dirichlet distributions to explain evidence. TBraTS then extended EC to medical image segmentation. Merging both Transformers and U-Net, TransUNet is a strong model for medical image segmentation. (2) Multi-task methods: (d) BCS [25] and (e) DSI [28]. The baseline of the Joint Classification and Segmentation framework (BCS) is a simple but useful way to share model parameters, which utilize two different encoders and decoders for learning respectively. The Deep Synergistic Interaction Network (DSI) has demonstrated superior performance in joint task. We adopt overall Accuracy (ACC) and F1 score (F1) as the evaluation criteria for the classification task. Dice score (DI) and Average Symmetric Surface Distance (ASSD) are chosen for the segmentation task.

Comparison with single- and multi-task methods. As shown in Table 1, we report the performance on the two datasets of the proposed UML and other methods. By comparison, we can observe the fact that the accuracy of

Table 2. The quantitative comparisons on the REFUGE dataset with vary NOISE levels.

REFUGE	0.030						0.050					
	CLS		SEG				CLS		SEG			
	<i>ACC</i>	<i>F1</i>	<i>DI_{disc}</i>	<i>ASSD_{disc}</i>	<i>DI_{cup}</i>	<i>ASSD_{cup}</i>	<i>ACC</i>	<i>F1</i>	<i>DI_{disc}</i>	<i>ASSD_{disc}</i>	<i>DI_{cup}</i>	<i>ASSD_{cup}</i>
BCS	0.620	0.694	<u>0.743</u>	<u>2.104</u>	<u>0.809</u>	<u>1.670</u>	0.430	0.510	<u>0.610</u>	<u>3.142</u>	<u>0.746</u>	<u>2.188</u>
DSI	<u>0.675</u>	<u>0.733</u>	0.563	9.196	0.544	9.705	<u>0.532</u>	<u>0.574</u>	0.409	8.481	0.364	9.794
Ours	0.827	0.857	0.830	1.752	0.840	1.407	0.733	0.785	0.744	2.142	0.778	2.009

the model results is low if either classification or segmentation is done in isolation, the ACC has only just broken 0.5 in EC. But joint classification and segmentation changes this situation, the performance of BCS and DSI improves considerably, especially the ACC and the Dice score of optic cup. Excitingly, our UML not only achieves the best classification performance in ACC (85.3%) and F1 (0.875) with significant increments of 1.8%, 4.9%, but also obtains the superior segmentation performance with increments of 6.6% in DI_{disc} and 3.2% in DI_{cup} . A similar improvement can be observed in the experimental results in ISPY-1.

Comparison under noisy data. To further valid the reliability of our model, we introduce Gaussian noise with various levels of standard deviations (σ) to the input medical images. The comparison results are shown in Table 2. As can be observed that, the accuracy of classification and segmentation significantly decreases after adding noise to the raw data. However, benefiting from the uncertainty-informed guiding, our UML consistently deliver impressive results. In Fig. 3, we show the output of our model under the noise. It is obvious that both the image-level uncertainty and the pixel-wise uncertainty respond reasonably well to noise. These experimental results can verify the reliability and interpre of the uncertainty guided interaction between the classification and segmentation in the proposed UML. The results of more qualitative comparisons can be found in the Supplementary Material.

Ablation Study. As illustrated in Table 3, both of the proposed UN and UI play important roles in trusted mutual learning. The baseline method is BCS. MD represents the mutual feature decoder. It is clear that the performance of classification and segmentation is significantly improved when we introduce supervision of mutual features. As we thought, the introduction of UN and UI takes the reliability of the model to a higher level.

4 Conclusion

In this paper, we propose a novel deep learning approach, UML, for joint classification and segmentation of medical images. Our approach is designed to improve the reliability and interpretability of medical image classification and segmentation, by enhancing image-level and pixel-wise reliability estimated by evidential deep learning, and by leveraging mutual learning with the proposed UN and

Table 3. The result of Ablation Study.

MD	UN	UI	CLS		SEG			
			<i>ACC</i>	<i>F1</i>	<i>DI_{disc}</i>	<i>ASSD_{disc}</i>	<i>DI_{cup}</i>	<i>ASSD_{cup}</i>
✓			0.765	0.810	0.835	<u>1.454</u>	<u>0.841</u>	<u>1.423</u>
✓	✓		0.813	0.845	<u>0.836</u>	1.333	0.826	1.525
✓		✓	<u>0.828</u>	<u>0.856</u>	0.786	1.853	0.823	1.593
✓	✓	✓	0.853	0.875	0.855	1.560	0.858	1.251

UI modules. Our extensive experiments demonstrate that UML outperforms baselines and introduces significant improvements in both classification and segmentation. Overall, our results highlight the potential of UML for enhancing the performance and interpretability of medical image analysis.

Acknowledgements: This work was supported by the National Research Foundation, Singapore under its AI Singapore Programme (AISG Award No: AISG2-TC-2021-003), A*STAR AME Programmatic Funding Scheme Under Project A20H4b0141, A*STAR Central Research Fund, the Science and Technology Department of Sichuan Province (Grant No. 2022YFS0071 & 2023YFG0273), and the China Scholarship Council (No. 202206240082).

References

1. Abdar, M., Samami, M., Mahmoodabad, S.D., Doan, T., Mazouze, B., Hashemifesharaki, R., Liu, L., Khosravi, A., Acharya, U.R., Makarenkov, V., et al.: Uncertainty quantification in skin cancer classification using three-way decision-based bayesian deep learning. *Computers in biology and medicine* **135**, 104418 (2021)
2. Chen, J., Lu, Y., Yu, Q., Luo, X., Adeli, E., Wang, Y., Lu, L., Yuille, A.L., Zhou, Y.: Transunet: Transformers make strong encoders for medical image segmentation. *arXiv preprint arXiv:2102.04306* (2021)
3. Cui, Y., Deng, W., Chen, H., Liu, L.: Uncertainty-aware distillation for semi-supervised few-shot class-incremental learning. *arXiv preprint arXiv:2301.09964* (2023)
4. Gal, Y., Ghahramani, Z.: Dropout as a bayesian approximation: Representing model uncertainty in deep learning. In: *international conference on machine learning*. pp. 1050–1059. PMLR (2016)
5. Han, Z., Zhang, C., Fu, H., Zhou, J.T.: Trusted multi-view classification. *arXiv preprint arXiv:2102.02051* (2021)
6. Harouni, A., Karargyris, A., Negahdar, M., Beymer, D., Syeda-Mahmood, T.: Universal multi-modal deep network for classification and segmentation of medical images. In: *2018 IEEE 15th International Symposium on Biomedical Imaging (ISBI 2018)*. pp. 872–876. IEEE (2018)
7. Jsang, A.: *Subjective logic: A formalism for reasoning under uncertainty*. Springer Verlag (2016)
8. Kang, Q., Lao, Q., Li, Y., Jiang, Z., Qiu, Y., Zhang, S., Li, K.: Thyroid nodule segmentation and classification in ultrasound images through intra-and inter-task consistent learning. *Medical image analysis* **79**, 102443 (2022)

9. Kim, T., Lee, H., Kim, D.: Uacanet: Uncertainty augmented context attention for polyp segmentation. In: Proceedings of the 29th ACM International Conference on Multimedia. pp. 2167–2175 (2021)
10. Kohl, S., Romera-Paredes, B., Meyer, C., De Fauw, J., Ledsam, J.R., Maier-Hein, K., Eslami, S., Jimenez Rezende, D., Ronneberger, O.: A probabilistic u-net for segmentation of ambiguous images. *Advances in neural information processing systems* **31** (2018)
11. Lakshminarayanan, B., Pritzel, A., Blundell, C.: Simple and scalable predictive uncertainty estimation using deep ensembles. *Advances in neural information processing systems* **30** (2017)
12. Mehta, S., Mercan, E., Bartlett, J., Weaver, D., Elmore, J.G., Shapiro, L.: Y-net: joint segmentation and classification for diagnosis of breast biopsy images. In: Medical Image Computing and Computer Assisted Intervention–MICCAI 2018: 21st International Conference, Granada, Spain, September 16-20, 2018, Proceedings, Part II 11. pp. 893–901. Springer (2018)
13. Newitt, D., Hylton, N., et al.: Multi-center breast dce-mri data and segmentations from patients in the i-spy 1/acrin 6657 trials. *Cancer Imaging Arch* **10**(7) (2016)
14. Orlando, J.I., Fu, H., Breda, J.B., Van Keer, K., Bathula, D.R., Diaz-Pinto, A., Fang, R., Heng, P.A., Kim, J., Lee, J., et al.: Refuge challenge: A unified framework for evaluating automated methods for glaucoma assessment from fundus photographs. *Medical image analysis* **59**, 101570 (2020)
15. Ronneberger, O., Fischer, P., Brox, T.: U-net: Convolutional networks for biomedical image segmentation. In: Medical Image Computing and Computer-Assisted Intervention–MICCAI 2015: 18th International Conference, Munich, Germany, October 5-9, 2015, Proceedings, Part III 18. pp. 234–241. Springer (2015)
16. Sensoy, M., Kaplan, L., Kandemir, M.: Evidential deep learning to quantify classification uncertainty. *Advances in neural information processing systems* **31** (2018)
17. Sensoy, M., Kaplan, L., Kandemir, M.: Evidential deep learning to quantify classification uncertainty. In: Proceedings of the 32nd International Conference on Neural Information Processing Systems. pp. 3183–3193 (2018)
18. Smith, L., Gal, Y.: Understanding measures of uncertainty for adversarial example detection. arXiv preprint arXiv:1803.08533 (2018)
19. Srivastava, N., Hinton, G., Krizhevsky, A., Sutskever, I., Salakhutdinov, R.: Dropout: a simple way to prevent neural networks from overfitting. *The journal of machine learning research* **15**(1), 1929–1958 (2014)
20. Thomas, S.M., Lefevre, J.G., Baxter, G., Hamilton, N.A.: Interpretable deep learning systems for multi-class segmentation and classification of non-melanoma skin cancer. *Medical Image Analysis* **68**, 101915 (2021)
21. Van Amersfoort, J., Smith, L., Teh, Y.W., Gal, Y.: Uncertainty estimation using a single deep deterministic neural network. In: International conference on machine learning. pp. 9690–9700. PMLR (2020)
22. Wang, J., Zheng, Y., Ma, J., Li, X., Wang, C., Gee, J., Wang, H., Huang, W.: Information bottleneck-based interpretable multitask network for breast cancer classification and segmentation. *Medical Image Analysis* **83**, 102687 (2023)
23. Wang, M., Lin, T., Wang, L., Lin, A., Zou, K., Xu, X., Zhou, Y., Peng, Y., Meng, Q., Qian, Y., et al.: Uncertainty-inspired open set learning for retinal anomaly identification. arXiv preprint arXiv:2304.03981 (2023)
24. Wang, X., Jiang, L., Li, L., Xu, M., Deng, X., Dai, L., Xu, X., Li, T., Guo, Y., Wang, Z., et al.: Joint learning of 3d lesion segmentation and classification for explainable covid-19 diagnosis. *IEEE transactions on medical imaging* **40**(9), 2463–2476 (2021)

25. Yang, X., Zeng, Z., Yeo, S.Y., Tan, C., Tey, H.L., Su, Y.: A novel multi-task deep learning model for skin lesion segmentation and classification. arXiv preprint arXiv:1703.01025 (2017)
26. Zhang, M., Xu, S., Piao, Y., Shi, D., Lin, S., Lu, H.: Preynet: Preying on camouflaged objects. In: Proceedings of the 30th ACM International Conference on Multimedia. pp. 5323–5332 (2022)
27. Zhou, Y., Chen, H., Li, Y., Liu, Q., Xu, X., Wang, S., Yap, P.T., Shen, D.: Multi-task learning for segmentation and classification of tumors in 3d automated breast ultrasound images. *Medical Image Analysis* **70**, 101918 (2021)
28. Zhu, M., Chen, Z., Yuan, Y.: Dsi-net: deep synergistic interaction network for joint classification and segmentation with endoscope images. *IEEE Transactions on Medical Imaging* **40**(12), 3315–3325 (2021)
29. Zou, K., Tao, T., Yuan, X., Shen, X., Lai, W., Long, H.: An interactive dual-branch network for hard palate segmentation of the oral cavity from cbct images. *Applied Soft Computing* **129**, 109549 (2022)
30. Zou, K., Yuan, X., Shen, X., Chen, Y., Wang, M., Goh, R.S.M., Liu, Y., Fu, H.: Evidencecap: Towards trustworthy medical image segmentation via evidential identity cap. arXiv preprint arXiv:2301.00349 (2023)
31. Zou, K., Yuan, X., Shen, X., Wang, M., Fu, H.: Tbrats: Trusted brain tumor segmentation. In: *Medical Image Computing and Computer Assisted Intervention–MICCAI 2022: 25th International Conference, Singapore, September 18–22, 2022, Proceedings, Part VIII*. pp. 503–513. Springer (2022)

Supplementary Materials

1. Parameters selection for w^m, w^c, w^s

Table S1. The process of parameters selection.

$0.5 * \mathcal{L}_{cls}$	$0.4 * \mathcal{L}_{seg}$	$0.1 * \mathcal{L}_{mut}$	CLS		SEG			
			<i>ACC</i>	<i>F1</i>	<i>DI_{disc}</i>	<i>ASSD_{disc}</i>	<i>DI_{cup}</i>	<i>ASSD_{cup}</i>
✓			<u>0.840</u>	<u>0.858</u>	0.031	63.992	0.000	78.304
✓	✓		0.805	0.836	<u>0.771</u>	<u>1.925</u>	<u>0.805</u>	<u>3.604</u>
✓	✓	✓	0.853	0.875	0.855	1.560	0.858	1.251

2. More visualizations

2.1 Additional visual results

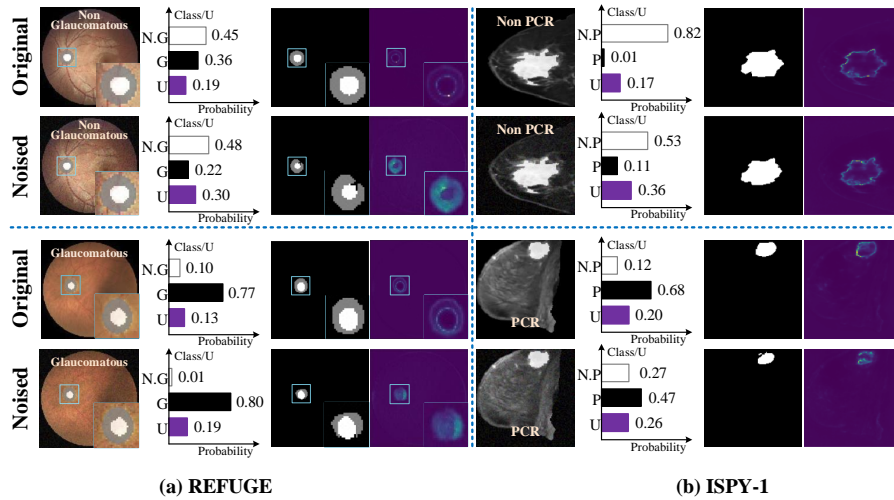


Fig. S1. Four additional visual results of segmentation and classification in REFUGE and ISPY-1. Top is the original image, and bottom is the input with Gaussian noise ($\sigma = 0.05$). From left to right, input (with GT), the result of classification (belief and image-level uncertainty), the result of segmentation, pixel-wise uncertainty.

2.2 Attention maps of classification

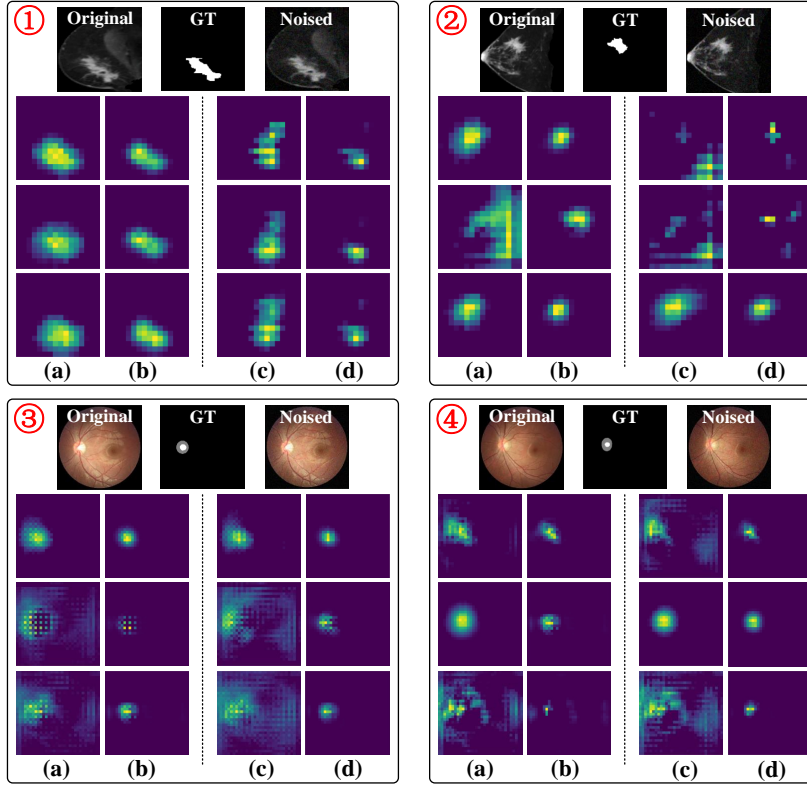


Fig. S2. The attention map of classification in REFUGE and ISPY-1 whose inputs are original or noised ($\sigma = 0.05$) images. ① and ② are in ISPY-1. ③ and ④ are in REFUGE. (a), (b) represent the channel maps of f_c^4 and r^c of the original images. (c), (d) represent the channel maps of f_c^4 and r^c of the noised images. The three channel maps are extracted from 1024 feature maps, randomly.

2.3 Qualitative comparison with multi-task methods.

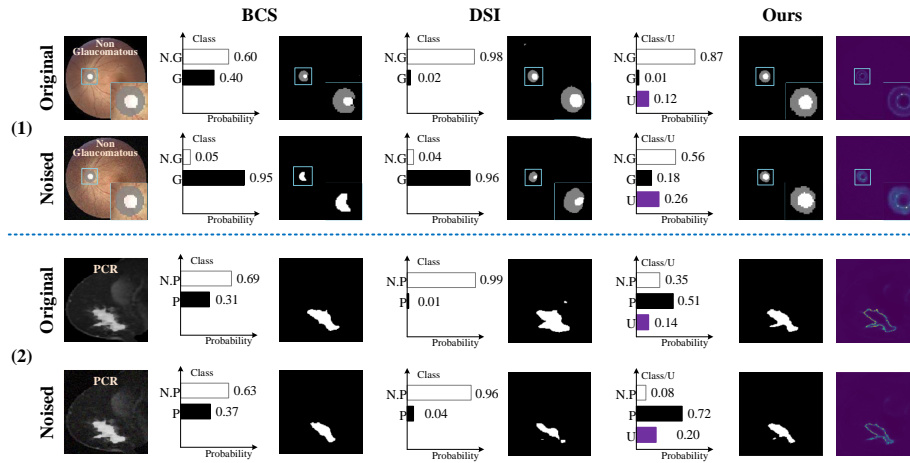


Fig. S3. The visual comparisons of classification and segmentation results in two datasets ((1) is REFUGE and (2) is ISPY-1) with multi-task methods.